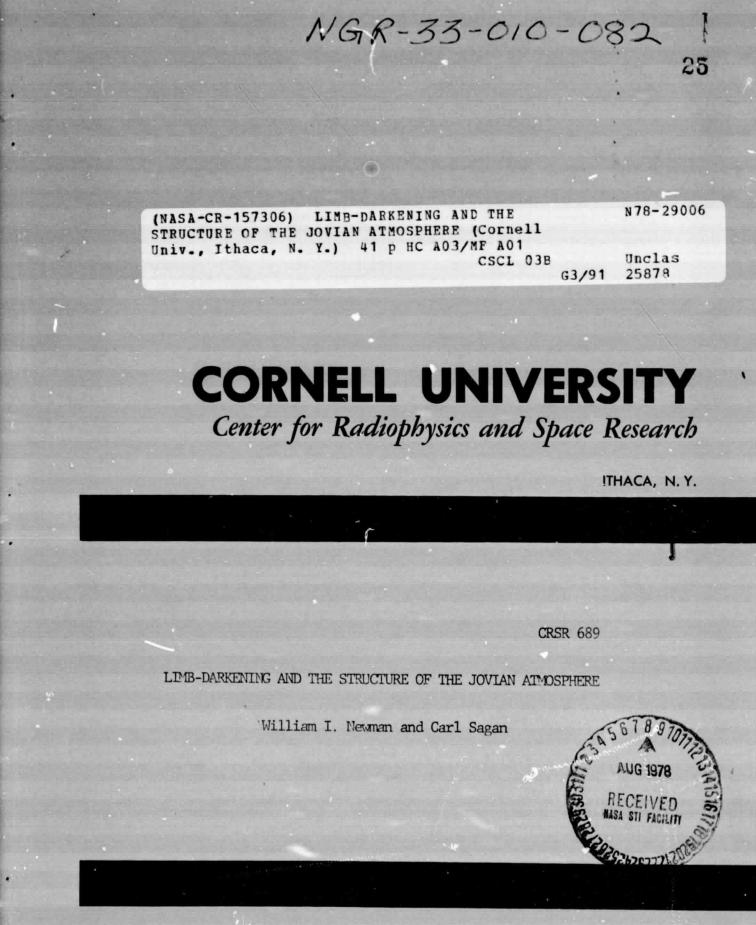
General Disclaimer

One or more of the Following Statements may affect this Document

- This document has been reproduced from the best copy furnished by the organizational source. It is being released in the interest of making available as much information as possible.
- This document may contain data, which exceeds the sheet parameters. It was furnished in this condition by the organizational source and is the best copy available.
- This document may contain tone-on-tone or color graphs, charts and/or pictures, which have been reproduced in black and white.
- This document is paginated as submitted by the original source.
- Portions of this document are not fully legible due to the historical nature of some of the material. However, it is the best reproduction available from the original submission.

Produced by the NASA Center for Aerospace Information (CASI)



LIMB-DARKENING AND THE STRUCTURE OF THE JOVIAN ATMOSPHERE

William I. Newman and Carl Sagan

Laboratory for Planetary Studies Cornell University Ithaca, New York 14853

٠.,

ABSTRACT

By observing the transit of various cloud features across the Jovian disk, Terrile and Westphal (1977) have constructed limb-darkening curves for three regions in the 4.6 to 5.1 µm band. Several models currently employed in describing the radiative or dynamical properties of planetary atmospheres are here examined to understand their implications for limb-darkening. The statistical problem of fitting these models to the observed data is reviewed and methods for applying multiple regression analysis are discussed. Analysis of variance techniques are introduced to test the viability of a given physical process as a cause of the observed limb-darkening.

The intermediate flux region of the North Equatorial Belt appears to be in only modest departure from radiative equilibrium. The limbdarkening curve for the South Temperate Belt is rich in structure and cannot be satisfactorily ascribed to any single physical mechanism; a combination of several, as yet unidentified, processes is likely involved. The hottest areas of the North and South Equatorial Belts exhibit limbdarkening curves that are typical of atmospheres in convective equilibrium. In this case, we derive a measure of the departure of the lapse rate from the dry adiabatic value ($n\approx 1.68$), which furnishes strong evidence for a phase transition at unit optical depth in the NEB and SEB. Although the system NH₃ -H₂S cannot be entirely ruled out, the freezing of an aqueous ammonia solution is shown to be consistent with the parameter fit <u>and</u> solar abundance data, while being in close agreement with Lewis' (1969a) cloud models.

i

I. INTRODUCTION

By applying a combination of radiative transfer and statistical techniques to infrared observations of Jupiter, we can enhance our understanding of the radiative and dynamical processes that control the make-up of the Jovian clouds and the deeper atmosphere. Since Jupiter's atmosphere is widely believed to be significantly stratified in its spectroscopically active components, observations made over limited wavelength regions permit us to look down at levels in the atmosphere where those components play an active role. Moreover, by analyzing the intensity observed in different regions of the disk, some of the underlying physics of Jupiter's belts and zones can be revealed.

The 5 µm region is of particular interest since it is transparent to the abundant Jovian absorbers, gaseous hydrogen, methane and ammonia. Gillett <u>et al</u>., (1969) observed that the 5 µm brightness temperature, averaged over a large part of the Jovian disk, was approximately 230° K. This value is much higher than most workers had expected and, since it corresponds to deep atmospheric levels, was a stimulus to further investigations. Westphal (1969), in observations of the North Equatorial Belt, showed that the 5 µm flux was coming from localized hot spots with brightness temperatures $>300^{\circ}$ K. He concluded that, if it is assumed that the cloud layer was near the top of the convective zone, the radiation was coming from below the clouds. Keay <u>et al</u>., (1973) and Westphal <u>et al</u>., (1974) produced high resolution maps of Jupiter confirming the existence of localized hot spots. In addition, they observed a correlation of 5 µm features with visual features in color photography. High thermal flux seemed to come from "blue" or "purple" regions whereas "orange" or "red" regions were not sources of intense 5 μ m radiation. They speculated that this dichotomy was likely due to the absence or presence of middle altitude red clouds. Sagan (1971) had earlier proposed that the blue coloration was due to Rayleigh scattering at roughly the 1 bar level when our view is not impeded by intervening clouds of red chromophores. Westphal <u>et al</u>. concluded (by studying the flux emanating from the shadow of Io as it passed across the Jovian disk) that the 5 μ m flux was not reflected or scattered sunlight but a genuine feature of radiative sources deep within Jupiter's atmosphere.

To better understand the nature of some of Jupiter's 5 µm features, Terrile and Westphal (1977) measured limb-darkening by selecting a region of interest and measuring its brightness as it rotated around the planet. In particular, they observed the hottest emitting areas of the North and South Equatorial Belts (with brightness temperatures of about 230 to 255° K), several bright 5 µm areas in the South Temperste Belt (with similar brightness temperatures), and intermediate flux regions in the North Equatorial Belt (with brightness temperatures near 240° K). This entailed the use of many different images of Jupiter taken over several hours in order to construct one limb-darkening curve. Notably, this technique did not suffer from the smearing effects of longitudinal inhomogeneities that would result from generating limb-darkening curves from thermal maps.

In parallel with these infrared observations, the atmosphere and composition of Jupiter was undergoing extensive study. Lewis (1969b) established that if the Jovian atmosphere possessed the solar abundance of water and annonia, the clouds were dominated by an aqueous annonia solution while the topmost cloud layer was solid annonia. He also showed that if sulfur were present in solar abundance, NH₄SH would form an important cloud layer. The infrared properties of liquid and solid water (Irvine and Pollack, 1968; Robertson and Williams, 1971) and annonia (Robertson and Williams, 1973; Robertson <u>et al.</u>, 1975) have been investigated at 5 μ m and are known to have very large absorption coefficients.

These 5 µm observations, together with predictions obtained from models of Jupiter's atmosphere and the infrared properties of its conjectured constituents, provide a compelling reason for analyzing the observed limb-darkening of various regions of the planet. In this communication, we present a combined radiative, dynamical and chemical model that reproduces the observed limb-darkening curves.

II. RADIATIVE AND DYNAMICAL MODELS

The plane-parallel approximation to the equation of radiative transfer is

$$\mu \frac{d}{d\tau} I(\tau,\mu) = I(\tau,\mu) - S(\tau)$$
(1)

where $\arccos \mu$ is the angle between the line of sight and the local planetary normal, τ is the optical depth, I is the intensity of the radiation and S is the source function. The optical depth is defined, in differential form, to be $d\tau = -\kappa dz$, where κ is the extinction coefficient, and z the altitude. All quantities in (1) are considered to have been modulated by the spectral response function of the InSb detector employed by Terrile and Westphal and integrated over the instrument's 4.6 to 5.1 µm bandwidth. Formally, (1) can be integrated to give the limb-darkening function.

$$I(0,\mu) = \frac{9}{5} S(\tau) \mu^{-1} \exp(-\tau/\mu) d\tau$$
 (2)

(Chandrasekhar, 1960). This equation is ideally suited to our analysis since Terrile and Westphal (1977) have evaluated $I(0,\mu)$. Thus, by inverting (2), we can determine the source function $S(\tau)$.

In general, the inversion is unique only if the limb-darkening function $I(0,\mu)$ has a known functional form. In the case of discrete data (particularly data contaminated by noise), the inversion is not unique and we must choose one of two approaches. In one approach, we calculate an approximate inversion kernel, K (τ,μ) , such that

$$S(\tau) \simeq \int K(\tau,\mu) I(0,\mu) d\mu$$
 (3)

(See the recent review article by Parker, 1977, for a description of "generalized inverse theory."). Combining (2) and (3), we require that

$$A(\tau,\tau') = \int_0^1 K(\tau,\mu) \mu^{-1} \exp((-\tau'/\mu) d\mu$$
 (4)

"approximate" the Dirac delta function, $\delta(t-t')$; that is, that the integral of A(t,t') over t or t' is unity and A(t,t') is strongly peaked when t' approaches t. The inversion is made complete by specifying the approximate source function and an estimate of the width of A(t,t') for different values of t (which, in turn, provides a measure of the characteristic convolutional smoothing evident in the approximate source function). Orton (1977) recently employed this technique in recovering the mean Jovian temperature structure from spectrally resolved thermal radiance data. This method, however, provides no direct insight into the physical processes that are the source of the infrared radiation and, moreover, has several mathematical deficiencies that are apparently not well-known (see Appendix I).

A less general but more physically motivated approach is to construct several radiative and dynamical models and obtain their corresponding source and limb-darkening functions. These models will depend, often nonlinearly, on a small number of parameters. By employing multiple regression methods, we then obtain numerical estimates of the parameters that are in a statistical sense most likely. By then employing analysis of variance techniques, we can assess whether the residual errors in the model fits are compatible with the experimental noise. This approach can demonstrate directly that a given physical model could be responsible for the observed limb-darkening while other models must be rejected. It is important to note that the fit obtained is most accurate for $\tau \approx 1$, the vicinity of the cloud tops and the region of greatest physical interest. The reason for this is clear from (2). The source function for $\tau>0$ depends strongly on $I(0,\mu)$ measured near the limb where instrumental accuracy is least. The source function for $\tau >>1$ is strongly attenuated and could vary significantly without seriously affecting the observed limb-darkening function. Because of the intuitive value of the method, we shall confine our attention to this technique and turn now to a discussion of models.

A. Power Series Expansion Model

Although the power series expansion

$$I(0,\mu) = \sum_{n=0}^{\infty} a_n \mu^n$$
 (5)

has no direct physical interpretation, we choose to include it for several

5

reasons. The truncated expansion was useful in an analysis of the limbdarkening of Venus (Goody, 1965; Newman, 1975). It can provide an estimate for the scatter in the data due to noise that is required in the analysis of variance. Finally, assuming that $I(0,\mu)$ is analytic and regular, the inversion of (2) can be performed directly giving (5) where the source function may be written

$$S(\tau) = \prod_{n=0}^{\infty} a_n \tau^n / n!$$
 (6)

In one instance, the well-known Eddington approximation, the truncated power series expansion is of special interest:

$$I(0,\mu) = I(0,0) (1 + 3/2\mu)$$
 (7)

This limb-darkening function results if the flux over the corresponding frequency passband is conserved. If the flux over the entire frequency spectrum is conserved, we have radiative equilibrium.

B. Convective Equilibrium Model

In our terrestrial experience, clouds are very efficient infrared absorbers of solar radiation as well as heat from the surface (additionally, in Jupiter's case, heat generated internally). A warmed parcel of gas will rise and adjust its pressure to that of its surroundings, the pressure of which varies according to the equation of hydrostatic equilibrium,

$$dP/dz = -\rho g \tag{8}$$

where P is the pressure, ρ the atmospheric mass density, and g the local gravitational acceleration. Thermal conduction times are very slow compared with dynamical times and may be neglected. Thus, the resulting

behavior of the parcel of gas is adiabatic and the pressure in the parcel behaves according to

$$\mathbf{P} = \tilde{\rho}^{\gamma}$$
 (9)

where $\tilde{\rho}$ is the parcel's mass density and γ is the ratio of specific heats.

Assuming that the absorbers responsible for the extinction are well-mixed with the principal atmospheric constituents, we can express the extinction coefficient as

$$\kappa = \sigma \mathbf{x} \rho / \mathbf{m}_{abs} \tag{10}$$

where σ is the cross-section to absorption, x is the mixing ratio of the absorbers to the principal atmospheric constituents, and m_{abs} is the mean mass of a single absorber molecule. Combining (2), (8), and (10), we obtain a linear dependence of pressure on optical depth, namely,

$$dP/d\tau = gm_{abs}/\sigma x \qquad (11)$$

By terrestrial analogy, we expect clouds to have a fairly sharp top at a level characterized by a temperature T_t and a pressure P_t . The discontinuous boundary may result from the transition from convective to radiative equilibrium or from phase changes. Defining τ to be zero above the cloud top (where we assume there to be no significant absorption), equation (11) is integrated as

$$P = P_{t} \left[1 + \frac{gm_{abs}}{\sigma xP_{t}} \tau \right]$$
 (12)

Pollack and Sagan (1965) derived a similar expression for the Venus atmosphere. In their case, however, the absorber was the principal atmospheric From (9) and the ideal gas law, we find

$$\frac{P}{P_{t}} = \begin{pmatrix} T \\ T_{t} \end{pmatrix}^{\frac{\gamma}{\gamma-1}} .$$
 (13)

Let us now assume that the clouds radiate as a black-body. By integrating the Planck function from 4.6 to $5.1 \mu m$ (assuming a relatively uniform response in the InSb interference filter employed by Terrile and Westphal), we obtain the approximate power-law dependence

Typical values for the exponent n are 12.3 and 11.6 for temperatures of 240°K and 250°K, respectively. Combining (12), (13), and (14) yields the intensity dependence on optical depth

$$B_{5\mu m}(\tau) = B_{5\mu m}(0) \left[1 + \frac{gm_{abs}}{\sigma xP_{t}}\tau\right] \frac{n(\gamma-1)}{\gamma}.$$
 (15)

If we combine the equation of state with (8) and (9), we obtain the dry adiabatic lapse rate

$$\frac{dT}{dz} = -\frac{m_{atm}}{k} \frac{\gamma - 1}{\gamma} g \qquad (16)$$

where m_{atm} is the mass of an atmospheric constituent and k is the Boltzmann constant. (For an inhomogeneous atmosphere, the meaning of an "atmospheric constituent" may be ambiguous. We define such a pseudo-particle as being characterized by a number-density weighted average of each component. In the terrestrial case, the mass of such a fictitious constituent would then be 0.78 the mass of N₂, 0.21.times the mass of O₂ and 0.01 the mass of a

trace constituent.) This equation indicates how the temperature of our parcel of gas decreases as it rises.

Suppose that the parcel of gas has a trace of a substance that is undergoing a phase transition, for example water vapor in the terrestrial atmosphere. As the vapor condenses, it evolves heat and precipitates out of the parcel. Because of latent heat it deposits in the parcel, the lapse rate is reduced. In particular (see Hess, 1959) the term $(\gamma-1)/\gamma$ in (15) and (16) should be replaced by $(\gamma-1)/n\gamma$, where n is given by

$$\eta = \frac{1 + \frac{\varepsilon L^2}{c_p k} \frac{W}{T^2}}{1 + \frac{LW}{kT}}$$
(17)

and c_p is the mean heat capacity of an atmospheric constituent, w the mixing ratio of condensates to atmospheric constituents, ϵ the ratio of the molecular weights of the condensates to that of the atmospheric constituents, and L the latent heat evolved by a single condensing molecule. Equation (16), when corrected for the condensate, defines the wet adiabatic lapse rate. Similarly, (15) becomes

$$B_{5\mu m}(\tau) = B_{5\mu m}(0) \left[1 + \frac{g m_{abs}}{\sigma x P_{t}} \tau \right] \frac{n(\gamma - 1)}{\gamma \gamma}$$
(18)

and describes the effective black body intensity as a function of optical depth for a wet adiabat.

Let us assume that the source function S(t) may be approximated by the effective black body intensity. For simplicity we write (18) as

$$S(\tau) = a(1+b\tau)^{c}$$
(19)

where a, b, and c correspond to appropriate terms in the previous equation. Then, employing (2), we find

$$I(0,\mu) = a(b\mu)^{\alpha} \exp \left[(b\mu)^{-1} \right] \Gamma \left[1+c, (b\mu)^{-1} \right]$$
 (20)

where Γ is the incomplete Gamma Function (Abramowitz and Stegun, 1965). A convenient formula for evaluating (20) is

$$I(0,\mu) = a(b\mu)^{c} \exp \left[(b\mu)^{-1} \right] \{ \Gamma \ (1+c) - \sum_{n=0}^{\infty} \frac{-(b\mu)^{-1}}{n! (c+1+n)} \}$$
(21)

where I here denotes the complete Gamma Function.

C. Cloud and Intermediate Zone Models

These models were employed by Terrile and Westphal (1977) in analyzing their data. Their cloud model describes radiation from an optically thick, hot cloud deck passing through an optically thin, warm, emitting layer. This may be represented by

$$I(0,\mu) = B_{\rm H} \exp(-\tau_{\rm w}/\mu) + B_{\rm w} \left[1 - \exp(-\tau_{\rm w}/\mu)\right]$$
(22)

where B_{H} and B_{W} are the black body radiation emitted from the hot and warm layers respectively, and τ_{W} is the optical depth of the warm layer. Radiation from an optically thick intermediate cloud deck passing through a cold absorbirg layer (I, intermediate model) may be represented as

$$I(0,\mu) = B_{T} \exp(-\tau_{T}/\mu)$$
 (23)

Both of these models can be expressed in the form

$$I(0,\mu) = a + b \exp(-\tau'/\mu)$$
 (24)

where the corresponding source function is given by

$$S(\tau) = \begin{cases} a & 0 \leq \tau^{<} \tau' \\ a + b & \tau' \leq \tau \end{cases}$$
 (25)

We do not expect these models to give particularly good fits because they require that each cloud and absorbing layer have a <u>uniform</u> temperature distribution. They are included, however, because they provide some insight into the nature of limb-darkening functions produced by atmospheres with relatively little temperature structure.

D. Thin Shell Model

It is also of interest to examine the limb-darkening function of an atmosphere characterized by the opposite extreme: an extremely hot, very thin emitter embedded at τ_0 in a warm, absorbing atmosphere. The source function used is

$$S(\tau) = a + b\delta(\tau - \tau_{a})$$
(26)

where δ is the Dirac delta function. The corresponding limb-darkening function is

$$I(0,\mu) = a + b\mu^{-1} \exp(-\tau_0/\mu) \qquad (27)$$

Although this model has no known physical counterpart, it provides a useful measure of the impact of strong temperature variation and pronounced thermal structure on the limb-darkening function.

Although our list of models is small, it describes a wide spectrum of behavior. The power series expansion describes virtually any continuous, smoothly varying limb-darkening function. Moreover, it can be used to provide an estimate of the scatter in the data due to noise. A special case of the polynomial is the Eddington approximation which provides an accurate representation of the limb-darkening curve when the radiative flux is conserved over a given passband, a hint of possible radiative equilibrium. We expect radiative equilibrium to be a dominant feature of high-elevation clouds (not under the influence of direct heating from the planet's interior) if dynamical effects are unimportant (a situation found to be the cas, on Venus by Newman, 1975). On the other hand, we expect that deeper clouds are dominated by dynamical effects and, from the suspected composition and temperature range of these clouds (Lewis, 1969b), subject to phase transitions in their spectroscopically active components. For this reason, we have emplus zed the derivation of the convective equilibrium model. Finally, as measures of the degree of thermal structure for the observed limbdarkening, we also consider Terrile and Westphal's (1977) cloud and intermediate zone models as well as a thin, extremely hot shell model. The source and limb-darkening functions for the different models are tabulated below.

statements and the second s

14

Model	Source Function	Limb-Darkening Function
Power-Series Expansion	n≝o an τ ⁿ /n!	n [#] o ^a n ^µ
Convective Equilibrium	а(1+bт) ^с	a (b _µ) ^{α} exp $\left[(b_µ)^{-1} \right] \Gamma \left[1+c, (b_µ)^{-1} \right]$
Cloud and Intermediate Zone	a, 0 ^{<} -τ ^{<} τ' a + b, τ' ^{<} τ	a+b exp(-τ'/μ)
Thin Shell	a+b δ(τ-τ _ο)	a+b μ ⁻¹ exp(-τ ₀ /μ)

Table 1. Limb-Darkening Properties of Various Models

III. STATISTICAL METHODS¹ AND ANALYSIS

Suppose we have N measurements, at various zenith angles (arccos μ_{i} , i = 1, ..., N) of the limb-darkening function (which we denote by I_{i}). For simple cases, a model may be considered composed of a linear combination of M different functions of μ , say $f_{i}(\mu)$; j = 1, ..., N. For example, a

1/ No single reference provides an adequate survey of this problem.

Relation (1965) reviews some of the numerical problems associated with least-squares techniques. Jenkins and Watts (1968) examine the theory of maximum likelihood estimators and Gaussian least squares as well as providing some remarks on nonlinear problems. Graybill (1968) considers the general linear model and some statistical tests of confidence. power series expansion employs the functions 1, μ , μ^2 , ..., μ^{M-1} and we make the identification $f_j(\mu) = \mu^{j-1}$. Nonlinear models will be treated later in this section. In addition, we assume that there is an additive Gaussian error noise component, e_i , whose mean vanishes and has a variance of σ^2 . Therefore, we write

$$\mathbf{I}_{i} = \sum_{j=1}^{M} \mathbf{i}_{j} \mathbf{f}_{j}(\mu_{i}) + \varepsilon_{i}, \quad i = 1, \dots, N \quad (28)$$

where the a_j are linear combination coefficients. We consider the error to be Gaussian distributed, a reasonable assumption from the Central Limit Theorem. Systematic errors, notably those due to calibration, are not Gaussian, and are often intractable.

Since the errors e_i defined by (28) are Gaussian distributed, the probability associated with the estimates of the a_i coefficients varies as

ехф	N -∑ i=1	$\epsilon_{i}^{2/\sigma^{2}}$	
-----	-------------------	-------------------------------	--

Therefore, the most probable choice of the coefficients is that which minimizes

$$\mathbf{U} = \sum_{i=1}^{N} \left[\mathbf{I}_{i} - \sum_{j=1}^{M} \mathbf{a}_{j} \mathbf{f}_{j}(\mathbf{u}_{i}) \right]^{2} \qquad (29)$$

The process of finding the values for the a_j coefficients is called the maximum likelihood method and is equivalent to the method of least squares. In this, the linear case, it is also known as the 'multiple regression' model. We therefore require that the derivative of U with respect to each a_i coefficient vanish, yielding the normal equations

$$\sum_{i=1}^{N} \mathbf{I}_{i} \mathbf{f}_{j}(\boldsymbol{\mu}_{i}) = \sum_{k=1}^{M} \mathbf{a}_{k} \left\{ \sum_{i=1}^{N} \mathbf{f}_{j}(\boldsymbol{\mu}_{i}) \mathbf{f}_{k}(\boldsymbol{\mu}_{i}) \right\} .$$
(30)

This set of linear equations is characterized by a matrix whose j_{k}^{k} component is given by

$$(\mathbf{f}_{j},\mathbf{f}_{k}) = \sum_{i=1}^{N} \mathbf{f}_{j} (\boldsymbol{\mu}_{i}) \mathbf{f}_{k} (\boldsymbol{\mu}_{i}) .$$
(31)

The matrix is symmetric, semi-positive definite and the system of equations has a unique solution unless one of the functions $f_j(\mu_i)$, evaluated at each μ_i , i = 1,...,N, could be represented by a linear combination of the remaining functions and is thus redundant.

Although superficially simple to solve, the system of linear equations (30) is numerically ill-conditioned. For example, an eighth degree polynomial fit to an arbitrarily large data set will result in the loss of twelve significant places of accuracy if a direct method (e.g., Gaussian elimination with pivoting) is used! To reduce this source of computational error, one should use Gram-Schmidt orthogonalization of the functions $f_j(\mu)$, j = 1, ..., M, with respect to the inner product operator defined in (31). The resulting matrix, associated with the normal equations will then be diagonal and the system's solution will then be trivial to obtain. A relatively recent innovation in solving least-squares problems is the technique of singular value decomposition. Although functionally equivalent to the Gram-Schmidt procedure, it is somewhat faster in execution. Moreover, unless posed in a certain form, the Gram-Schmidt procedure is susceptible to numerical instabilities.

15

े असल्पत्ति		SAR CODA	Contract of the				ŧ.							1		` I		5 5 3	1 71	
		1							1				-	* 1	1			1. I	· •	
Contraction of the local division of the loc	and states of the second	and the second second	9	Charles and the second s	 in the second second	م در در		in the set	te - officiated	in second second	an and a state of the	\$-market	لعوسدينهم			in Long ti	a decem			-

Singular value decomposition is a very complex procedure but is described in detail in Lawson and Hanson (1974) and Forsythe <u>et al.</u>, (1977). Also, both texts contain tested ANSI Standard Fortran programs.

Although the errors associated with an ideal experiment are independent of each other, the errors estimated by (28), where the a_j coefficients satisfy (30), are not. In fact, combining (28) and (30), we find

$$\sum_{i=1}^{N} \varepsilon_{i} f_{j}(\mu_{i}) = 0 \text{ for } j = 1, \dots, M \qquad . \tag{32}$$

So, although there are N values of ε_i , equations (32) introduce M conditions or constraints and we are left with N-M degrees of freedom. Moreover, if we calculate the expectation value of U (the sum of the residual variances) defined by (29), we can show that

$$\langle U \rangle = \sum_{i=1}^{N} \langle \varepsilon_i^2 \rangle = (N-M) \sigma^2$$
(33)

The least squares estimation processes introduce a small bias (which vanishes as the number of data points becomes arbitrarily large) due to (32) into our estimates of the ε_i . By increasing the number of a_j coefficients, equations (32) show that we reduce the noise level in each ε_i until the number of coefficients M equals the number of data points N and all ε_i vanish (i.e., the fit is exact). This, qualitatively, is the result shown by (33). We can approximate the latter by writing

$$\sigma^{2} = \frac{1}{N-M} \sum_{i=1}^{N} \varepsilon_{i}^{2}$$
(34)

(This result is exact <u>only</u> if we replace ε_i^2 by $\langle \varepsilon_i^2 \rangle$.) Suppose, for

example, that we know our limb-darkening function has an exact representation, apart from noise, as a polynomial of degree M'. Using (34), we can estimate σ^2 . If we fit the data with a polynomial of degree N>M', our estimate of σ^2 from (34) will remain approximately the same because the decrease in the noise level is <u>exactly</u> compensated for by the denominator N-M. However, if we use an estimate of the polynomial degree M<M', we will find that the residuals ε_i contain not only noise information but limb-darkening information as well, and our estimate of σ^2 will be too large.

Using (34) we can now define a χ^2 variable with N-M degrees of freedom, namely

$$\chi^{2} = \sum_{i=1}^{N} \epsilon_{i}^{2} / \sigma^{2} \qquad (36)$$

If σ^2 is known (i.e., we have an absolute estimate of our sources of error), we can employ the usual confidence-level tests.

If σ^2 is not known, the χ^2 test cannot be used. The problem of finding the polynomial degree M' is then complicated by the fact that (34) is an approximation. In practice, we find that σ^2 decreases with increasing M, until M equals M'. For larger M, the estimate of σ^2 tends to oscillate around a constant, making the task of identifying M' very difficult.

By modifying a technique developed by Akaike (1969) in application to autoregressive decomposition, we can construct a variable that will better equip us to estimate M'. We note that, as M increases, the a_j coefficients adapt to the properties of the noise in that experiment until the number of coefficients and data points are the same and no residual errors remain. Let us suppose that, next door to Terrile and Westphal, there was a competing group using equivalent instrumentation making the same observations at the same zenith angles. The underlying limb-darkening function would be the same for both groups but the noise observed presumably would not. (The errors of course, would be drawn from the same statistical population.) We then ask how well the a_j coefficients computed for Terrile and Westphal's observations would match their rivals' data. That is, if their competitors observed intensities I'_i , $i=1,\ldots,N$, how large would U_A be, where we define

$$U_{A} = \sum_{i=1}^{N} \left[I_{i} - \sum_{j=1}^{L} a_{j} f_{j}(\mu_{j}) \right]^{2}$$
(36)

A straightforward but tedious calculation reveals that

$$\langle U_A \rangle = (N+M) \sigma^2 = \frac{N+M}{N-M} \langle U \rangle$$
 (37)

when MMM'. As M increases beyond M', U_A (as an approximation to $\langle U_A \rangle$) <u>increases</u> because the surfeit of coefficients are adding to U_A some of the noise level observed in the first experiment. This variable U_A therefore provides a test of the universality of the fit. In practice, we can only estimate $\langle U_A \rangle$ by evaluating $\left[(N+M)/(N-M) \right] U$, for increasing values of M. The resulting locus of points is parabolic in character with M' corresponding to the minimum. Since we have obtained U_A (and not $\langle U_A \rangle$), the points may oscillate, but the uncertainty in M' is characteristically reduced. Finally, knowing M', we can estimate σ^2 from (34). This value, however, is not accurate enough to permit anything but the crudest χ^2 test of significance.

.

٠

.

As an illustration of these methods, we tabulate some relevant quantities for polynomials fitted to Terrile and Westphal's observations.

Polynomial Fit Results	Case A Equatorial Belt Hot Spots	Case B South Temperate Belt	Case C Intermediate Flux (NEB)		
N	100	50	24		
U 1st degree 2nd degree 3rd degree 4th degree 5th degree	0.1754 0.1370 0.1358 0.1323 0.1316	0.2181 0.1343 0.1327 0.1207 0.1097	0.04681 0.04677 0.03832 0.03667 0.03586		
o 1st degree 2nd degree 3rd degree 4th degree 5th degree	0.04230 0.03758 0.03761 0.03732 0.03742	0.06741 0.05346 0.05371 0.05179 0.04994	0.04613 0.04719 0.04377 0.04393 0.04463		
U _A 1st degree 2nd degree 3rd degree 4th degree 5th degree	0.1825 0.1455 0.1471 0.1462 0.1484	0.2363 0.1514 0.1558 0.1475 0.1397	0.05532 0.06010 0.05365 0.05598 0.05976		

Table	II.	Power	Series	Expansion	Parameters

In Case A, the Akaike criterion would clearly select a quadratic fit. The oscillation in U_A is not a hindrance here. In Case B, the minimum is

reached for a fifth degree polynomial. However, that fit (as well as the 6th, 7th and 8th order fits) extrapolates to a negative intensity at the limb and must be disregarded. We consider, accordingly, a quartic polynomial to be appropriate. Case C is somewhat ambiguous because of the strong oscillation in U_A . Although M=3 is a minimum, the corresponding a_j coefficients would provide a source function that was negative at $\tau = 1.41$ and must be excluded. Hence, the first degree polynomial is selected. It is important to note that, in this case, physical and not statistical considerations resolved the degree of the polynomial fit.

Nonlinear models are significantly more difficult to fit and analyze than their linear counterparts. Instead of linear combination coefficients a_j , we will employ parameters a_j , j = 1.2, ..., M, so that we can parallel equation (28) by writing

$$I_{i} = F(\mu_{i}; a_{1}, \dots, a_{M}) + \varepsilon_{i}$$
(38)

where the function F describes our model (such as the convective or cloud models). We define the residual variance U by

$$\mathbf{U} \equiv \sum_{i=1}^{N} \left[\mathbf{I}_{i} - \mathbf{F}(\boldsymbol{\mu}_{i}; \mathbf{a}_{1}, \dots, \mathbf{a}_{M}) \right]^{2} .$$
(39)

We perform a variation of the parameters a_j so as to minimize U, in compliance with the maximum likelihood principle. Unlike the linear case, there may be several minima and a global search must be performed.

The maximum likelihood estimates of the parameters a_j satisfy the normal equations (derived by differentiating U with respect to a_j),

$$\sum_{i=1}^{N} \mathbf{I}_{i} \frac{\partial F}{\partial \mathbf{a}_{j}} (\boldsymbol{\mu}_{i}; \mathbf{a}_{1}, \dots, \mathbf{a}_{M}) = \sum_{i=1}^{N} F(\boldsymbol{\mu}_{i}; \mathbf{a}_{1}, \dots, \mathbf{a}_{M}) \frac{\partial F}{\partial \mathbf{a}_{j}} (\boldsymbol{\mu}_{i}; \mathbf{a}_{1}, \dots, \mathbf{a}_{M})$$

$$j = 1, \dots, M \qquad (40)$$

.

The minimization of (39) or, alternatively, the solution of (40) is a very difficult computational problem (consider the convective model (21), for example). A survey of this problem may be found in Luenberger (1973).

As in the linear case, we have N measures of the error (38) and M constraints, equations (40). By linearizing $F(u; a_1, \ldots, a_n)$, we can demonstrate the approximate validity of (33)-(35) in the nonlinear problem. Thus, once we have obtained the maximum likelihood estimate of the a_j parameters, the statistical method of analysis is much the same as before. Because of nonlinearity, there is no direct analogue to Akaike's criterion.

In comparing the residual variances U for different models, we require, following (34), that they have the same number of parameters. Thus, the intermediate zone model may be compared with a first degree polynomial, and the convective equilibrium, thin shell or cloud models with a second degree polynomial. Higher order power series must be treated on an individual basis.

The residual variances U of the models considered are tabulated below.

Variance	Case A	Case B	Case C
Polynomial 1 Degree 2 3 4 5	0.1754 0.1370 0.1358 0.1323 0.1316	0.2181 0.1343 0.1327 0.1207 0.1097	0.04681 0.04677 0.03832 0.03668 0.03586
Convective	0.1371	0.1530	0.04683
Shell	0.1516	0.1344	0.04538
Cloud Layer	0.1444	0.1347	0,04556
Intermediate			0.05466

Table III. Summary of Fitted Results

For large N-M, the χ^2 statistic, using (35), defined by $(2\chi^2)^{\frac{1}{2}}$ -(2N - 2M - 1)^{$\frac{1}{2}$}, is approximately Gaussian distributed with vanishing mean and unit variance. Since we do not know σ^2 , we cannot employ the χ^2 test directly. However, the a. nature of the χ^2 distribution assures us that relative differences between model residual variances of only a few percent can be significant.

In Case A, the hot areas of the North and South Equatorial belts, the quadratic power series and the convective e_{4} uilibrium model provide almost equally reliable fits, while all other models are much less probable. The convective equilibrium fit (19) gave the parameters b and c values of 2.01 and 2.04 respectively. The value of b could be varied over a wide range (while that of c was adjusted in order to minimize U for a given b). However, the value of c did not change significantly. Since $c \approx 2$, the correspondence between the goodness of the quadratic and the convective equilibrium model fits is not unexpected. We discuss the physical implications of thus result in the next section.

The South Temperate Belt is more problematic. The investigation of power series expansions for Case B reveals a preference for a fit of high degree, indicating significant structure. The convective equilibrium model is clearly rejected. However, the other three-parameter models (the quadratic polynomial, the thin shell model and the cloud layer models) are equally likely, statistically! We can only conclude that the physical mechanism responsible for the behavior of the South Temperate Belt is an amalgam of several physical processes or a region of transition between two physical processes.

Finally, the intermediate flux region of the North Equatorial Belt allows for several models as possible mechanisms. The preferred degree of a polynomial fit is unity, as we have discussed earlier, while the addition of a quadratic term does not significantly change the results. The convective equilibrium model is viable and the associated parameter b can vary from 1.4 to 1.6 (while c ≈ 0.9) without significantly affecting the residual variance. Note that the Eddington approximation corresponds to b = 1.5 and c = 1.0. This is highly suggestive of flux conservation and radiative escilibrium. We also observe that the intermediate zone model of Terrile and Westphal is clearly rejected, while the thin shell and cloud layer models are approximately equally probable. The latter suggests that there is more thermal structure present than we normally associate with a state of radiative equilibrium.

23

Finally, let us consider how Lewis' (1969a, 1969b) model is consistent with these results. The hot spots have a brightness temperature of 250-255°K. This corresponds directly to the transition wegion from aqueous annonia to ice, suggesting that a phase change coupled through the high opacity of aqueous annonia (and the dynamic mixing that might arise from this low-lying cloud layer) to convective equilibrium may be present. The intermediate flux zone of the North Equatorial Belt is cooler and at a higher altitude. Since no phase transition is predicted and higher-level clouds are less likely to be dynamically coupled to what lies below, radiative equilibrium might be a reasonable approximation to the mechanism present. Finally, the South Temperate Belt remains an enigma. Since it appears to be fairly hot, it could be intermediate in structure between the other regions.

IV. CHEMISTRY OF PHASE TRANSITIONS

In Section III, we argued for a phase transition in the hot spots of Jupiter's equatorial belt. From the observation that the value of the convective equilibrium parameter c = 2.04 and the identification, from equations (18) and (19), that

$$c = n (\gamma - 1)/\mu\gamma , \qquad (47)$$

(cf. Pollack a & Sagan, 1965), we can now estimate n, the term defined by
(17) that shows the departure from a dry adiabat. We adopt n = 11.6.
We now assume that the aimosphere of Jupiter is 88.6% hydrogen and
11.2% helium, from Weidenschilling and Lewis (1973). This is consistent

24

with solar abundances and with the β Sco occultation data (Elliot et al., 1974), Pioneer 10 ultraviolet photometer data (Carlson and Judge, 1974), Pioneer 10 infrared radiometer data (Orton, 1975) and the infrared spectrum determination by Houck et al. (1975). A variation of 5% in our assumed He abundance will affect our results. through γ , only about 1%. A simple calculation then shows that $\gamma \simeq 1.42$. Combining these results, we find that $\mu \simeq 1.68$. The latent heats of water and ammonia are, respectively, 333.6 and 351 Joules per gram (International Critical Tables, 1928), Now, neither water nor armonia will freeze at 250°K and the corresponding (Sagan and Salpeter, 1976) $P \approx 2$ bars (water freezes at a higher temperature and amnonia at a lower one). If they could, equation (17) would provide for mixing ratios of 0.0452 and 0.0494. These values are 5.35 and 42.8 times the estimates given by Weidenschilling and Lewis for solar abundance. Since, for clouds, we expect to find an excess of the spectroscopically active materials, these excess values are not excluded.

A mixture of water and ammonia, however, provides for a large range of freezing points. (See Zemansky, 1963 and C. stellan, 1971 for a discussion of cutectic curves and freezing mixtures.) The cutectic properties of aqueous ammonia solutions were investigated over half a century ago by Potsma (1920) and Elliott (1924). At low temperatures, water does not readily dissociate in the presence of ammonia to form ammonium hydroxide. Anmonia can, however, form two hydrates, $NH_3 \cdot H_20$ and $NH_3 \cdot 2H_20$ by hydrogen bonding. The two hydrates also exist on the freezing point diagram. Therefore, depending on the strength of the initial aqueous ammonia solution, the sequence in which freezing takes place can be very complex. Moreover, unlike the laboratory situation, the behavior in the Jovian atmosphere is considerably complicated by precipitation. Water is denser than ice which is denser than frozen annonia which is denser than liquid annonia (Kuiper, 1952). So, once the temperature drops to that on the eutectic curve, one of the four active constituents (H_2O , $NH_3 \cdot 2H_2O$, $NH_3 \cdot H_2O$, NH_3) will begin to freeze and either rise or sink faster than the mixture. The depletion of this constituent from the solution changes its concentration and lowers its associated freezing point. As the solution is buoyed higher by convection, it further cools and loses more of one of its constituents. As a result, the freezing point can be smeared out over as much as $100^{\circ}K$ (for the $NH_3 - NH_3 \cdot H_2O$ system). Since the latent heats of fusion for water and amnonia are quite weak, the latent heats of the two hydrates should not be significantly changed and this picture remains unaltered.

Water and ammonia vapors are relatively poor absorbers from 4.6 to 5.1 µm. Moreover, as we expect both ammonia and frozen ammonia to form above the water or ice clouds (from the above buoyancy arguments and Lewis, 1969b), we expect that it would be very difficult to see down to the water or ice clouds at this wavelength. [Perhaps most water vapor that exists above the water clouds readily dissolves in the ammonia clouds and immediately freezes out. Since we expect large-scale moist convection to occur below this level (Gierasch, 1976), the amount of water vapor present at lower levels will depend on whether we are seeing a convective updraft or downdraft. In the case of a downdraft, the large-scale convective model predicts the presence of very little water vapor. The reduction in the expected absorption from water vapor in the downdraft would result in observations of much deeper and hotter levels in the Jovian atmosphere. The combination, then, of a freeze-out mechanism at higher levels and convective downdrafts below could explain Larson et al.,'s (1975) unexpectedly low water vapor abundance and high observed brightness temperature.]

٩

.

The possibility of hydrogen sulfide playing a major role in convective equilibrium models cannot definitely be excluded. Unlike water, H_2S readily dissociates in annonia. Moreover, all attempts to freeze such mixtures in laboratories have produced many compounds of annonia and hydrogen sulfide. The eutectic curve for the NH_3 — H_2S system is incompletely known and appears to have at least one incongruent melting point (Scheflan and McCrosky, 1932); in addition the relevant latent heats have not been tabulated. For a reasonable estimate of the latent heat, the required mixing ratios are far in excess of that predicted from solar abundances. If hydrogen sulfide, however, is not well-mixed in the atmosphere, its role in the chemistry and coloration of the hot spots cannot be discounted (cf. Khare and Sagan, 1975).

Although carbon monoxide has recently been detected in the 5 μ m band in the Jovian atmosphere (Beer, 1975), it is unlikely that CO could be responsible for Terrile and Westphal's observations. It is believed to be formed deep in the atmosphere (Larson <u>et al.</u>, 1978). In the temperature range of interest, it can be expected to react with molecular hydrogen and to form methane (which is transparent at 5 μ m) and water. Moreover, to fit the convective equilibrium wet-addabat model, carbon monoxide would have to undergo a phase change near 250^OK and would

necessarily be many tens or hundreds of times more abundant than solar values would suggest.

The analysis techniques of the present paper should be applicable to high-spatial resolution multi-frequency limb-darkening scans of Jupiter with the Voyager spacecraft (Hanel, <u>et al.</u>, 1978) -- which can potentially clarify much about the lateral and vertical structure, chemistry and cloud constituents of the Jovian atmosphere.

Acknowledgment

We are grateful for stimulating discussions to Peter Gierasch, E. E. Salpeter, William Forrest, Adam Devir, B. N. Khare, R. Treffers and Freeman Dyson.

This research was supported by NASA Grant NCR 33-010-082.

Abramowitz, M. and Stegun, I. A. (1965). <u>Handbook of Mathematical</u> Functions, Superintendent of Documents, Washington.

Akaike, H. (1969). Fitting autoregressive models for prediction. Ann. Inst. Statist. Math. 21, 243-247.

Beer, R. (1975). Detection of Carbon Monoxide in Jupiter, <u>Ap</u>. J. Lett. 200, L167-L169.

- Carlson, R. W. and Judge, D. L. (1974). Pioneer 10 ultraviolet photometer observations at Jupiter encounter, J. Geophys. Res. 79, 3623-3633.
- Castellan, G. W. (1971). <u>Physical Chemistry</u>, Addison-Wesley, Reading, Mass.

Chandrasekhar, S. (1960), Radiative Transfer, Dover, New York.

- Conrath, B. J. (1972). Vertical Resolution of Temperature Profiles Obtained from Remote Radiation Measurements, <u>J. Atmos. Sci., 29</u>, 1262-1271.
- Elliot, J., Wasserman, L. H., Veverka, J., Sagan, C., and Liller, W. (1974). The occultation of Beta Scorpii by Jupiter. II. The hydrogen-helium abundance in the Jovian atmosphere, <u>Astrophysics</u> J. 190, 719-729.
- Elliott, L. D. (1924). The Freezing Point Curve of the System Water-Ammonia, J. Phys. Chem., 28, 887-888.
- Forsythe, G. E., Malcolm, M. E. and Noler, C. B. (1977). Computer Methods for Mathematical Computation, Prentice-Hall, Englewood-Cliffs, pp. 192-239.

٠

Foster, M. (1961). An Application of the Wiener-Kolmogorov Scoothing Theory to Matrix Inversion, J. Soc. Indust. Appl. Math. 9, 387-392.

- Gierasch, P. J. (1976). Jovian Meteorology: Large-Scale Moist Convection, Icarus 29, 445-454.
- Gillett, F. C., Low, F. J. and Stein, W. A. (1969). The 2.8—14 Micron Spectrum of Jupiter, Astrophys. J. 157, 925-934.
- Goody, R. M. (1965). The structure of the Venus cloud veil, J. Geophys. Res. 70, 5471-5481.
- Graybill, F. A. (1976). <u>Theory and Application of the Linear Model</u>, Duxbury Press, North Scituate, Mass.
- Hanel, R., Conrath, B., Gautier, D., Gierasch, P., Kumar, S., Kunde, V., Lowman, P., Maguire, W., Pearl, J., Pirraglia, J., Ponnamperuma, C., and Samuelson, R. (1978). The Voyager Infrared Spectroscopy and Radiometry Investigation, Space Science Revs., in press.
- Hess, S. L. (1959). Introduction to Theoretical Meteorology, Holt, Rinehart and Winston, New York.
- Houck, J. R., Schaack, D., Reed, R. A., Pollack, J. and Summers, A. (1975). Jupiter: its infrared spectrum from 16 to 40 microns, Science 189, 720-722.
- International Critical Tables (1928). McGraw-Hill, New York,
- Irvine, W. M. and Pollack, J. B. (1968). Infrared Optical Properties of Water and Ice Spheres, Icarus 8, 324-360.
- Jenkins, G. M. and Watts, D. G. (1968). Spectral Analysis and Its Applications, Holden-Day, San Francisco.
- Keay, C. S. L., Low, F. J., Rieke, G. H. and Minton, R. B. (1973). High-Resolution Maps of Jupiter at Five Microns, Astrophys. J. 183, 1063-1073.

Khare, B. N. and Sagan, C. (1975). Cyclic Octatomic Sulfur: A Possible Infrared and Visible Chromophore in the Clouds of Jupiter, Science 189, 722-723.

₹

- Kuiper, G. P. (1952). Planetary Atmospheres and Their Origin, in The <u>Atmospheres of the Earth and Planets</u> (Revised Edition), G. P. Kuiper, editor, U. of Chicago Press, Chicago.
- Larson, H. P., Fink, U., Treffers, R. and Gautier, T. N. III (1975). Detection of Water Vapor on Jupiter, <u>Astrophys. J. 197</u>, L137-L140.
- Larson, H. P., Fink, U. and Treffers, R. R. (1978). Evidence for CO in Jupiter's Atmosphere from Airborne Spectroscopic Observations at 5 Microns, Ap. J. 219, 1084-1092.
- Lawson, C. W. and Hanson, R. J. (1974). Solving Least Squares Problems, Prentice-Hall, Englewood-Cliffs.
- Lewis, J. S. (1969a). Observability of Spectroscopically Active Compounds in the Atmosphere of Jupiter. <u>Icarus 10</u>, 393-409.
- Lewis, J. S. (1969b). The Clouds of Jupiter and the NH₃-H₂O and NH₃-H₂S Systems, <u>Icarus 10</u>, 365-378.
- Luenberger, D. G. (1973). Introduction to Linear and Non-Linear Programming, Addison-Wesley, Reading, Mass.
- Newman, W. I. (1975). Infrared Limb Darkening of the Venus Atmosphere, Icarus 26, 451-456.
- Orton, G. S. (1975). The thermal structure of Jupiter. I., <u>Icarus 26</u>, 125-141.
- Orton, G. S. (1977). Recovery of the Mean Jovian Temperature Structure from Inversion of Spectrally Resolved Thermal Radiance Data, Icarus 32, 41-57.

Parker, R. L. (1977). Understanding Inverse Theory, Ann. Rev. Earth Planet, Sci., 5, 35-64.

- Pollack, J. B. and Sagan, C. (1965). The Infrared Limb-Darkening of Venus, J. Geophys. Res. 70, 4403-4426.
- Potsma, S. (1920). Le Systeme Annoniaque-Eau, Rec. Trav. Chim., 39, 515-536.
- Ralston, A. (1965). A First Course in Numerical Analysis, McGraw-Hill, New York.
- Robertson, C. W., Downing, H. D., Carnutte, B. and Williams, D. (1975). Optical constants of solid annonia in the infrared, J. Opt. Soc. Am. 65, 432-435.
- Robertson, C. W. and Williams, D. (1971). Lambert Absorption Coefficient of Water in the Infrared, J. Opt. Soc. Am. 61, 1316-1320.
- Robertson, C. W. and Williams, D. (1973). Optical constants of liquid ammonia in the infrared, J. Opt. Soc. Am. 63, 188-193.
- Sagan, C. (1971). The Solar System Beyond Mars, Space Science Revs. 11, 73-112.
- Sagan, C. and Salpeter, E. E. (1976). Particles, Environments and Hypothetical Ecologies in the Jovian Atmosphere, Astrophys. J. Suppl. 32, 737-755.
- Sagan, C., Veverka, J., Wasserman, L., Elliot, J., and Liller, W. (1974). Jovian Atmosphere: Structure and Composition between the Turbopause and the Mesopause, Science 184, 901-903.
- Schoflan, L. and McCrosky, C. R. (1932). A Phase Study of the System Annonia-Hydrogen Sulfide, J. Amer. Chem. Soc. 54, 193-202.
- Terrile, R. J. and Westphal, J. A. (1977). The Vertical Cloud Structure of Jupiter from 5 µm Measurements, Icarus 30, 274-281.

- Weidenschilling, S. J. and Lewis, J. S. (1973). Atmospheric and Cloud Structures of the Jovian Planets, Icarus 20, 465-476.
- Westphal, J. A. (1969). Observations of Localized 5-Micron Radiation from Jupiter, Astrophys. J. 157, L63-L64.
- Westphal, J. A., Matthews, D. and Terrile, R. J. (1974). Five-Micron Pictures of Jupiter, Astrophys. J. 188, L111-L112.

Zemansky, M. W. (1968). Heat and Thermodynamics, McGraw Hill, New York.

APPENDIX I

Orton (1977) employed Conrath's (1972) formulation of the Backus-Gilbert generalized inverse theory. In the discrete case in the absence of noise, the method can be stated quite succinctly. Consider the problem of best approximating some function $\Delta T(x)$ given m observations ΔI_4 defined by

$$\Delta \mathbf{I}_{i} = \int_{0}^{\mathbf{x}} \mathbf{k}_{i}(\mathbf{x}) \ \Delta \mathbf{T}(\mathbf{x}) d\mathbf{x}, \qquad \mathbf{i} = 1, \dots, \mathbf{m} \qquad . \tag{I-1}$$

(We adhere strictly to Conrath's notation. The discussion that follows, however, is independent of the choice of the limits of integration, provided they are finite.) We then wish to construct an approximate inverse $\widehat{\Delta T(x)}$ from a linear combination of the observed data, namely

$$\widehat{\Delta \mathbf{T}(\mathbf{x})} = \sum_{i=1}^{m} \mathbf{a}_{i}(\mathbf{x}) \Delta \mathbf{I}_{i}$$
(I-2)

where we have yet to specify a rule for selecting $a_i(x)$. If we define a function A(x,x') by

$$A(\mathbf{x},\mathbf{x}') = \sum_{i=1}^{m} a_i(\mathbf{x}) k_i(\mathbf{x}') , \qquad (I-3)$$

we see that

$$\widehat{\Delta T(\mathbf{x})} = \int_{0}^{\mathbf{x}} A(\mathbf{x},\mathbf{x}') \Delta T(\mathbf{x}') d\mathbf{x}' \qquad . \qquad (I-4)$$

The function A(x,x'), ideally, should tend to a Dirac δ -function. In practice, it will have a finite width or spread and tends to smooth $\Delta T(x)$. For this reason, it is called an "averaging kernel." In order to estimate the width of A(x,x'), we define a "spread function" s(x) by

$$s(x) = 12 \int_{0}^{x} (x-x')^{2} A^{2}(x,x') dx' , \qquad (1-5)$$

We then perform a variation on s(x) in order to minimize the "spread," subject to the normalization constraint

$$1 = \int_{0}^{x} A(x,x') dx' , \qquad (I-6)$$

The factor 12 in equation (I-5) is introduced so that, if A(x,x') is a rectangle of unit area and width w, s(x) = w. This variation can most simply be achieved using Lagrange multipliers (Conrath, 1972).

The method is conceptually attractive since it will provide the estimate of $\Delta T(x)$ with what seems to be the best possible resolution. Although the method can be of significant value in certain applications, it suffers from important mathamatical shortcomings which can seriously affect its performance. In the absence of any further information about the physical processes involved, two mathematical principles must be employed when devising an <u>ad hoc</u> inversion scheme. First, <u>all</u> available information must be incorporated into the method so that the solution obtained reproduces the available data. Second, the method must yield increased resolution over other approaches.

The variational procedure employed in estimating $a_i(x)$ never uses the information obtained by the observations (I-1) as equations of constraint. As a result, the approximate inverse $\widehat{\Delta T(x)}$ will not, in general, reproduce the observed data ΔI_i . By not fully introducing the observational information available into the method, we compound our ignorance of the solution. The second problem arises in the determination of the resolution or, alternatively, the spread. Although, s(x) reproduces reasonably well the width of a number of functions, it can give spurious results when applied to some degenerate kernels. Consider, for example, a hypothetical experiment where we measure ΔI_i defined by

$$\Delta I_{i} = \int_{-1}^{1} P_{i-1}(x) \Delta T(x) dx, \quad i = 1, ..., m \quad (I-7)$$

where $P_i(x)$ is the ith Legendre polynomial. Let us select $a_i(x)$ and, therefore, $\widehat{\Delta T(x)}$ to be given by

$$a_{i}(x) = \frac{2i-1}{2}P_{i-1}(x)$$
(I-8)
$$\widehat{\Delta T(x)} = \sum_{i=1}^{m} \frac{2i-1}{2}P_{i}(x)\Delta I_{i}$$

(In many circumstances, we customarily make this choice of expansion since it provides the best approximation, in an integrated least-squares sense, to a given function.) Although Conrath's variational procedure would not make this identification for $a_i(x)$, it is instructive to consider the spread function that results from this choice.

Now, the averaging kernel becomes

$$A(x,x') = \sum_{\ell=0}^{m-1} \frac{2\ell+1}{2} P_{\ell}(x) P_{\ell}(x') \qquad . \qquad (I-9)$$

(We know, incidentally, from the completeness relation for Legendre polynomials that this kernel "tends" to a Dirac δ -function.) Using the

recurrence relation

$$(\ell+1)P_{\ell+1}(x) - (2\ell+1)xP_{\ell}(x) + \ell P_{\ell-1}(x) = 0 , \qquad (I-10)$$

we obtain the Christoffel-Darboux identity

$$A(x,x') = \frac{m}{2} \left[\frac{P_{m}(x)P_{m-1}(x') - P_{m}(x')P_{m-1}(x)}{x - x'} \right] .$$
 (I-11)

Then, using (I-5) with integration limits -1 to 1, we observe that

$$S(x) = 6m^{2} \left[\frac{P_{m-1}(x)}{2m+1} + \frac{P_{m}^{2}(x)}{2m-1} \right]$$
(I-12)

and the average spread $\langle s(x) \rangle$ is

$$\langle \mathbf{s}(\mathbf{x}) \rangle = \frac{1}{2f} \mathbf{s}(\mathbf{x}) \, d\mathbf{x}$$
 . (I-13)
 $= \frac{12m^2}{4m^2 - 1}$

This result shows that the average spread <u>increases</u> as we add more terms (and corresponding data points) and, as m approaches infinity, reaches a limiting value of 3 (which is larger than the region over which we are calculating the spread). The measure of spread that we use must show increased resolution as we increase the number of data points and, in the limit of an infinite amount of available information or data, must tend to zero. The spread function of (I-5) is incompatible with these conceptual requirements. Although we have shown that the spread function (I-5) can be a misleading indicator of resolution, it is important to understand in practical terms why this is so. The morphology of a typical averaging kernel is characterized by a central peak, for x near x', and some kind of "sid-lobe" structure. Theoretical kernels (e.g., rectangles, Gaussians, etc.) for which (I-5) is a reasonable measure of spread have no sidelobes. The kind of kernel more likely to be encountered in practice will have a complex sidelobe structure. If these sidelobes do not decay much faster than $(x-x')^{-1}$, they will provide a significant if not dominant contribution to the spread function (I-5). In practice, the highly oscillatory character of the sidelobes tends to cause cancellations and diminish any sizeable contribution. However, since (I-5) contains the <u>square</u> of th kernel, this cancelling feature of the sidelobes is lost and their effects are grossly exaggerated.

•

.

This form of generalized inverse theory, then, has two serious drawbacks. It will not reproduce the given data and can provide a very spurious estimate of the resolution of the result. For completeness, we cite an approximate inversion formula (see, for example, Foster, 1961) that satisfies

$$\int_{0}^{\mathbf{x}} \mathbf{k}_{\mathbf{i}}(\mathbf{x}) \left\{ \widehat{\Delta \mathbf{T}(\mathbf{x})} - \Delta \mathbf{T}(\mathbf{x}) \right\} d\mathbf{x} = 0 \quad \mathbf{i} = 1, \dots, \mathbf{m} \quad ; \quad (\mathbf{I} - \mathbf{14})$$

that is, any error in our approximate inverse cannot be seen from available observational data. We define a matrix C by its i, j components

$$C_{i,j} = \int_{0}^{x} k_{i}(x) k_{j}(x) dx \quad i,j = 1,...,m \quad . \quad (I-15)$$

Then,

$$a_{i}(x) = \sum_{j=1}^{m} \begin{bmatrix} c^{-1} \end{bmatrix}_{i,j} k_{j}(x)$$

$$A(x,x') = \sum_{\substack{i,j=1 \\ i,j=1}}^{m} \begin{bmatrix} c^{-1} \end{bmatrix}_{i,j} k_{i}(x) k_{j}(x') , \quad (I-16)$$

$$T(x) = \sum_{\substack{i,j=1 \\ i,j=1}}^{m} \begin{bmatrix} c^{-1} \end{bmatrix}_{i,j} I_{i}k_{j}(x)$$

where $\begin{bmatrix} C^{-1} \end{bmatrix}_{i,j}$ denotes the i, jth component of the inverse matrix to C.